Quantum Monte Carlo study of correlation energy and pair correlation function at various electron-positron density ratios: Accurate calculation of positron annihilation lifetimes in solids

Y. Dong,* L. Deng,* Y. H. Li, M. Luo, J. D. Liu, H. J. Zhang,† and B. J. Ye‡
State Key Laboratory of Particle Detection and Electronics, University of Science and Technology of China, Hefei 230026, China

(Received 8 July 2023; revised 7 December 2023; accepted 7 February 2024; published 4 March 2024)

Positron annihilation lifetime spectroscopy is a unique technique to probe the defect structure of crystalline solids. To distinguish different defect states, accurate calculation of the positron annihilation lifetimes is demanded to compare with the experimental results. We perform quantum Monte Carlo calculations to compute the electron-positron correlation energy and pair correlation function at several electron-positron density ratios. This approach enables us to obtain new fitting parameters under the local density approximation to combine with two-component density functional theory to calculate the positron lifetimes of defect-free bulk and monovacancy defects in various materials. As compared with the experimental results, this method outperformed some previous schemes and provided theoretical support for the previous deduction of certain vacancy defects.

DOI: 10.1103/PhysRevB.109.104104

I. INTRODUCTION

Positron annihilation lifetime spectroscopy (PALS) is a powerful technique to investigate the defect structures of crystalline solids [1,2] and the porous structure of polymeric and supermicroporous materials [3,4]. To distinguish different defect types in crystalline solids, it is key to compare different calculated positron annihilation lifetimes with the analysis results of PALS experiments [5,6]. Therefore, accurate calculation of the positron annihilation lifetimes is highly meaningful and necessary for the defect study of materials.

Two-component density functional theory (TCDFT) has been widely utilized to calculate positron parameters of positron lifetime and Doppler broadening of annihilation radiation in solids due to its computation efficiency and high accuracy [5,7,8]. Among the physical quantities of TCDFT calculation, the electron-positron correlation potential and the pair correlation function (PCF) play key roles to affect the correctness of the results. Several TCDFT calculation schemes, including the conventional scheme (CONV, proposed by Boronski *et al.* [8]), the GGGC scheme (proposed by Gilgien, Galli, Gygi, and Car [9]), and the PSN scheme (proposed by Puska, Seitsonen, and Nieminen [10]), have been widely used and performed well [11]. These schemes, which differ slightly in the fitting form of the correlation energy and pair correlation function, are all based on data of several decades ago by Arponen *et al.* [12] and Lantto *et al.* [13].

In 2011, Drummond and his collaborators performed a quantum Monte Carlo (QMC) study for a positron in electron gas and obtained a new form of correlation functional with the local density approximation (LDA) [14]. The QMC results were further corrected by the generalized gradient approximation (GGA) method [15] and then applied to DFT study to compute positron lifetimes which are closer to the experimental values [16,17]. In 2022, Simula *et al.* used QMC directly to simulate an electron-positron wave function instead of using DFT, and successfully computed the positron lifetimes in crystalline C, Si, Li, and AlN [18]. These studies demonstrate the potential of QMC to calculate positron lifetimes more accurately. They were all very suitable to calculate the positron lifetimes in defect-free materials. Most recently, Deng *et al.* utilized QMC to simulate a full LDA correlation functional to successfully calculate the contact magnetic fields in muon spin relaxation (μ^+SR) technology [19]. Inspired by this, to calculate positron lifetimes more accurately, especially for the vacancy-type defects, we attempted QMC simulations to obtain a full LDA electron-positron correlation functional including the electron-positron correlation potential and PCF.

In this work, a QMC study was carried out at different positron densities in electron gas by using CASINO [20]. The LDA was applied by assuming that all interaction energy terms only depend on the local densities of positrons and electrons. Then the electron-positron correlation energy and PCF could be derived. Since the PSN scheme is also a computational approach that utilizes a full LDA electron-positron correlation functional, we adopted the form of the correlation energy function of the PSN scheme and performed parameter fitting using the data from the QMC study. The correlation functional was then applied to the positron lifetime calculation by TCDFT. In brief, the QMC data in 2011 [14] were limited to the zero-positron-density approximation and the derived positron lifetimes of vacancy-type defects wait for the improvement of accuracy, while the current TCDFT calculations relied on older raw data [12,13]. So, in this study, we obtained new parameters of full LDA electron-positron correlation energy and PCF using QMC, and combined them with lattice relaxation to achieve improved computational results for perfect lattices and vacancy-type defects.

*These authors contributed equally to this work.
†hjzhang8@ustc.edu.cn
‡bjye@ustc.edu.cn

II. TCDFT SYSTEM

In 1930, Dirac proved that when the relative velocity v between a positron and an electron is much smaller than the speed of light c, the annihilation rate λ of 2γ annihilations per unit time is given by

$$\lambda = \pi r_e^2 c n_e, \tag{1}$$

where r_e is the classical electron radius and n_e is the electron density at the positron annihilation site. This implies that the annihilation rate is directly proportional to the density of positrons and electrons. Therefore, to calculate the positron annihilation lifetime, it is necessary to obtain the density distribution of the electron-positron system from the wave function. Calculating the total wave function of the system is challenging. For the practical applications, in the independent particle model (IPM), positrons and electrons are often treated as independent particles. Therefore, the wave function of a two-particle system can be written as the product of the positron wave function and the electron wave function. Subsequently, an enhancement factor $\gamma(\mathbf{r}, [n_e, n_p])$ (n_p is positron density) is introduced for the correlation effects between the particles at the annihilation site within the local density approximation [8]. In this approximation method, the annihilation rate can be expressed as

$$\lambda = \pi r_e^2 c \int d\mathbf{r} n_e(\mathbf{r}) n_p(\mathbf{r}) \gamma(\mathbf{r}, [n_e, n_p]). \tag{2}$$

The enhancement factor can be deduced by the PCF, which stands for the enhancement from one-body density to true two-body density. One can use the following equations to define the PCF:

$$\rho_{pe}(\mathbf{r}, \mathbf{r}') = n_p(\mathbf{r}) n_e(\mathbf{r}') g_{pe}(\mathbf{r}, \mathbf{r}') \tag{3}$$

or

$$\rho_{pe}(\mathbf{r}, \mathbf{r}') = \frac{\int \Psi^*(\mathbf{r}, \mathbf{r}', \mathbf{r_3}, \ldots, \mathbf{r_N}) \Psi(\mathbf{r}, \mathbf{r}', \mathbf{r_3}, \ldots, \mathbf{r_N}) d\mathbf{r_3} \ldots d\mathbf{r_N}}{\int \Psi^*(\mathbf{r_1}, \mathbf{r_2}, \ldots, \mathbf{r_N}) \Psi(\mathbf{r_1}, \mathbf{r_2}, \ldots, \mathbf{r_N}) d\mathbf{R}}, \tag{4}$$

where ρ_{pe} is the diagonal element of the positron (p) and electron (e) two-particle density matrix, Ψ is the many-body wave function, and g_{pe} is the PCF. Here, within the LDA, we are truly interested in the zero-distance enhancement of a homogenous system with densities n_e and n_p, which means the contact density enhancement of the positrons and electrons, $g_{pe}[\mathbf{r_e} = \mathbf{r_p}, n_e(\mathbf{r_e}), n_p(\mathbf{r_p})]$, namely, $g[0; n_e(\mathbf{r}), n_p(\mathbf{r})]$ or $g(0)$. One can define that

$$\gamma(\mathbf{r}, [n_e, n_p]) = g[0; n_e(\mathbf{r_e}), n_p(\mathbf{r_p})]. \tag{5}$$

Within the framework of TCDFT, the total energy can be written as

$$E[n_e, n_p] = E[n_e] + E[n_p] + \int d\mathbf{r} V_{\text{ext}}(\mathbf{r})[n_e(\mathbf{r}) - n_p(\mathbf{r})] - \int d\mathbf{r} \int d\mathbf{r}' \frac{n_e(\mathbf{r}) n_p(\mathbf{r}')}{|\mathbf{r} - \mathbf{r}'|} + E_{\text{corr}}^{e-p}[n_e, n_p], \tag{6}$$

where $E[n_e]$ and $E[n_p]$ are the one-component functionals of the electrons and positrons, V_{ext} is an external potential, and E_{corr}^{e-p} is an electron-positron correlation functional. The fundamental equation to obtain the one-body wave function for the electrons (the Kohn-Sham equation [21]) is

$$\left[-\tfrac{1}{2}\nabla^2 - \phi(\mathbf{r}) + V_{xc}^- + V_c^-\right]\psi^- = \epsilon^-\psi^-, \tag{7}$$

and for positrons, it is

$$\left[-\tfrac{1}{2}\nabla^2 + \phi(\mathbf{r}) + V_{xc}^+ + V_c^+\right]\psi^+ = \epsilon^+\psi^+, \tag{8}$$

where $\phi(\mathbf{r})$ is the sum of the total Hartree potential and the external due to nuclei, which can be written as

$$\phi(\mathbf{r}) = \int d\mathbf{r}' \frac{n_p(\mathbf{r}') - n_e(\mathbf{r}')}{|\mathbf{r} - \mathbf{r}'|} - V_{\text{ext}}(\mathbf{r}). \tag{9}$$

V_{xc} is the exchange correlation potential between the electrons or positrons. V_c is the correlation potential between the positrons and electrons, which can be expressed as

$$V_c^{\pm} = \frac{\delta E_{\text{corr}}^{e-p}[n_p, n_e]}{\delta n_{p,e}}. \tag{10}$$

Except for the electron-positron correlation energy and enhancement factor, all of the above-mentioned physical quantities are relatively well established. Therefore, the key issue is to obtain a sufficiently accurate correlation energy and enhancement factor. To summarize, using TCDFT, the positron and electron wave functions will be obtained by solving Eqs. (7) and (8), and then the annihilation rate can be calculated using Eq. (2). The electron-positron correlation energy and enhancement factor used for the TCDFT calculation were obtained through the QMC method exhibited in the following section.

III. QMC STUDY OF THE PCF AND CORRELATION ENERGY

Within the LDA, the correlation energy and PCF are only related to the local density of the electrons and the positrons. Therefore, homogeneous gas systems for positrons and electrons are simulated.

A Slater-Jastrow-backflow (SJB) [22,23] trial wave function is used with plane-wave orbits,

$$\psi_{PW}^{\text{SJB}} = e^{J(\mathbf{R})}\{\phi_i[\mathbf{r}_\downarrow^- + \xi(\mathbf{R})]\}\{\phi_j[\mathbf{r}_\uparrow^- + \xi(\mathbf{R})]\} \times \{\phi_I[\mathbf{r}_\uparrow^+ + \xi(\mathbf{R})]\}\{\phi_J[\mathbf{r}_\downarrow^+ + \xi(\mathbf{R})]\}, \tag{11}$$

where $J(\mathbf{R})$ is the Jastrow exponent and $\xi(\mathbf{R})$ is the backflow displacement (only the u term is used in the Jastrow exponent), $\mathbf{R}$ are the positions of all the particles, ϕ is the plane-wave basis, $\mathbf{r}_\downarrow^-(\mathbf{r}_\downarrow^+)$ and $\mathbf{r}_\uparrow^-$ $(\mathbf{r}_\uparrow^+)$ are the positions of up and down spin electrons (positrons), respectively, and $\{\cdot\}$ denotes a Slater determinant; more details can be found in Appendix A. In a real annihilation event, only one positron is present. However, for simulation purposes involving different ratios of positrons and electrons, it becomes necessary to use multiple positrons. Therefore, we are employing a nonpolarized particle model for the simulation, which means there are equal spin-up and spin-down positrons in the system. We would like to find out how much difference there is between the results of QMC and the previous results. Furthermore, the simulations in this study using a plane-wave basis are only tailored for high-density scenarios. The simulation results may

not be applicable to very low-density situations; further study in this aspect is required.

The variational Monte Carlo (VMC) variance-minimum scheme [24] is first used to optimize the Jastrow exponents. After that, backflow optimization is applied and, finally, a diffusion Monte Carlo (DMC) calculation is performed. The DMC time step is set to 0.001, 0.002, and 0.003 a.u. The target population of walkers of DMC is 1500. The final results for the pair correlation function (PCF) are the mean value of three time steps, while the final results of correlation energy are obtained by performing a linear fit on the results from three different time steps [14] and the final $g(0)$ is calculated by $2g_{\mathrm{DMC}}(0) - g_{\mathrm{VMC}}(0)$ [25].

Within the PSN scheme (the form of the electron-positron correlation functional assumes symmetry with respect to the density of the positron and electron), the enhancement factor can be expressed as [8]

$$g(0; n_e, n_p) = a(n_e)n_p^3 + b(n_e)n_p^2 + c(n_e)n_p + g_0(n_e) \quad \text{for } n_p \leqslant n_e \text{ (swap } n_e \text{ and } n_p \text{ if } n_e \leqslant n_p), \tag{12}$$

where $a(n)$, $b(n)$, and $c(n)$ can be described by the PCFs g_0, g_1, and g_2 with three particular positron-electron density ratios ($R = n_p/n_e$): $R \to 0$, $R = 1$, and $R = \frac{1}{2}$, respectively:

$$\begin{aligned} a(n) &= \frac{1}{n^3}[2k(n) - 6g_1(n) + 8g_2(n) - 2g_0(n)], \\ b(n) &= \frac{1}{n^2}[-3k(n) + 11g_1(n) - 16g_2(n) + 5g_0(n)], \\ c(n) &= \frac{1}{n}[k(n) - 4g_1(n) + 8g_2(n) - 4g_0(n)], \end{aligned} \tag{13}$$

where

$$k(n) = \frac{1}{2}n\frac{d}{dn}g_1(n). \tag{14}$$

Meanwhile, the electron-positron correlation energy [10] can be expressed as

$$\frac{1}{E_{c,v}^{e-p}[n_p, n_e]} = a\left(r_s^e\right) + b\left(r_s^e\right)r_s^p + c\left(r_s^e\right)\left(r_s^p\right)^2 + \frac{4\pi}{3}\frac{\left(r_s^p\right)^3}{\epsilon_0\left(r_s^e\right)} + \frac{4\pi}{3}\frac{\left(r_s^e\right)^3}{\epsilon_0\left(r_s^p\right)}, \tag{15}$$

where r_s^e (r_s^p) is the electron (positron) density parameter defined by $n_e = \frac{3}{4\pi(r_s^e)^3}$ ($n_p = \frac{3}{4\pi(r_s^p)^3}$). ϵ_0 is the correlation energy of one positron (electron) in a homogeneous electron (positron) gas. The parameters a, b, and c can be expressed as

$$\begin{aligned} a\left(r_s^e\right) &= A_a + B_a r_s^e + C_a\left(r_s^e\right)^2, \\ b\left(r_s^e\right) &= B_a + B_b r_s^e + C_b\left(r_s^e\right)^2, \\ c\left(r_s^e\right) &= C_a + C_b r_s^e + C_c\left(r_s^e\right)^2. \end{aligned} \tag{16}$$

Based on the above information, three different density ratios of positrons and electrons, $R \to 0$, $R = \frac{1}{2}$, and $R = 1$, are chosen to perform QMC simulations. The specific numbers of positrons and electrons selected for the three density ratios are as follows: ($N_p = 1, N_e = 64$), ($N_p = 30, N_e = 60$), and ($N_p = 40, N_e = 40$). The correlation energy data obtained at $R = 1$ and $R = \frac{1}{2}$ are used to fit the six parameters that appear in the electron-positron correlation energy formula. Since the simulation of $R \to 0$ has been performed by Drummond [14] and our results are in good agreement with theirs, we will directly utilize their fitting formulas later.

The data points of time step 0.001 a.u. are shown in Table I as an example, while $g(0)$ is the final result. Among them, the PCF data for the 1:64 density ratio show good agreement with the results obtained from Drummond [14]. The finite-size error is discussed in Appendix B. After considering the low-density limit and Kimball cusp conditions [26], the raw data are processed as discussed in Appendix A; the contact PCF data are then well represented by

$$g_1 = 1 + 1.3005r_s - 0.3089r_s^2 - 0.0776r_s^{2.5} + \frac{r_s^3}{6}, \tag{17}$$

$$g_2 = 1 + 1.8353r_s - 0.7687r_s^2 + 0.1313r_s^{2.5} + \frac{r_s^3}{6}, \tag{18}$$

and g_0 can be expressed the same as in Drummond's work [14]:

$$g_0 = 1 + 1.23r_s - 3.38208r_s^{3/2} + 8.6957r_s^2 - 7.37037r_s^{7/3} + 1.75648r_s^{8/3} + 0.173694r_s^3, \tag{19}$$

where $r_s = (\frac{3}{4\pi n})^{1/3}$. The PCF data are obtained with a time step of 0.001 a.u. The DMC calculation for the three density ratios is shown in Fig. 1. In Fig. 1(d), $g(0)$ of $R = 1$ and $R = \frac{1}{2}$ is larger than that of the PSN scheme after $r_s^e = 3$, while $g(0)$ of $R \to 0$ is smaller than that of the PSN scheme. This means that the new values of $g(0)$ will be more concentrated. This will have a significant impact on the lifetime calculations, especially for vacancy defects.

For the positron-electron correlation energy, both the energy data points obtained from $R = 1$ ($N_e = 40, N_p = 40$) and $R = \frac{1}{2}$ ($N_e = 60, N_p = 30$) are used to fit the six parameters in Eqs. (15) and (16). These data points are shown in Table II and can be calculated by

$$E_{c,v}^{e-p} = E_v(N_e + N_p) - E_v(N_e) - E_v(N_p), \tag{20}$$

where $E_{c,v}^{e-p}$ is the electron-positron correlation energy per volume and E_v is the energy per volume. The fitted curve is shown as a dashed line in Fig. 2, while the solid line represents the data from the PSN scheme. Although the differences between them are small, there are still noticeable discrepancies, especially for r_s^e values between 1 and 3. The fitted parameter results are as follows (ϵ_0 from Drummond's work [14] is used):

$$\begin{aligned} aa &= 2.379, \quad ba = -4.498, \quad ca = -0.400, \\ bb &= 13.610, \quad cb = -10.810, \quad cc = 2.910. \end{aligned} \tag{21}$$

The new correlation energy and the PSN correlation energy as functions of the positron density n_p (at $r_s^e = 2, 3, 4, 5$) are shown in Fig. 3. The dashed lines are the QMC results and the solid lines are the PSN results. The values of the former are noticeably larger than those of the latter. Indeed, this will clearly have a significant impact on the subsequent calculation of positron annihilation lifetimes. It is important to note that our QMC simulations were only performed for r_s^e values ranging from 1 to 8. Therefore, the data obtained are

TABLE I. Data points obtained from quantum Monte Carlo (QMC) simulations with a time step of 0.001 a.u., except for the final results of $g(0)$ (average results of the time steps of 0.001, 0.002, and 0.003). The error of $g(0)$ is obtained from fitting, $r_s^e = (\frac{3}{4\pi n_e})^{1/3}$. N_e and N_p are the numbers of electrons and positrons in QMC simulations. r_s^e is in a.u. (Bohr). $E_{\rm VMC}$, $E_{\rm DMC}$, Error of $E_{\rm DMC}$ and Var. of VMC are in a.u. (Hartree) per particle.

r_s^e	N_e	N_p	$E_{\rm VMC}$	Var. of VMC	$E_{\rm DMC}$	Error of $E_{\rm DMC}$	$g(0)$	Error of $g(0)$
1	40	40	0.4928	2.7751	0.4883	0.00009	1.850	0.0251
2	40	40	−0.0516	0.6152	−0.0547	0.00004	3.226	0.0338
3	40	40	−0.1115	0.3230	−0.1146	0.00003	5.505	0.0688
4	40	40	−0.1187	0.2437	−0.1223	0.00005	9.774	0.0598
5	40	40	−0.1163	0.2062	−0.1207	0.00005	16.062	0.1834
6	40	40	−0.1113	0.2015	−0.1170	0.00002	26.637	0.1210
1	60	30	0.4323	1.3252	0.4286	0.00009	1.932	0.0103
2	60	30	−0.0541	0.2969	−0.0568	0.00004	3.598	0.0458
3	60	30	−0.1060	0.1419	−0.1086	0.00002	6.373	0.0517
4	60	30	−0.1113	0.0986	−0.1144	0.00005	11.267	0.0464
5	60	30	−0.1079	0.0834	−0.1115	0.00005	19.179	0.2008
6	60	30	−0.1035	0.1161	−0.1077	0.00005	31.194	0.1705
1	64	1	0.5560	0.9561	0.5536	0.00008	2.107	0.0314
2	64	1	−0.0067	0.1810	−0.0082	0.00004	4.087	0.0554
3	64	1	−0.0719	0.0643	−0.0730	0.00004	7.347	0.0714
4	64	1	−0.0809	0.0346	−0.0818	0.00003	12.729	0.2732
5	64	1	−0.0784	0.0231	−0.0792	0.00004	22.744	0.3128
6	64	1	−0.0735	0.0159	−0.0743	0.00002	35.303	0.2830

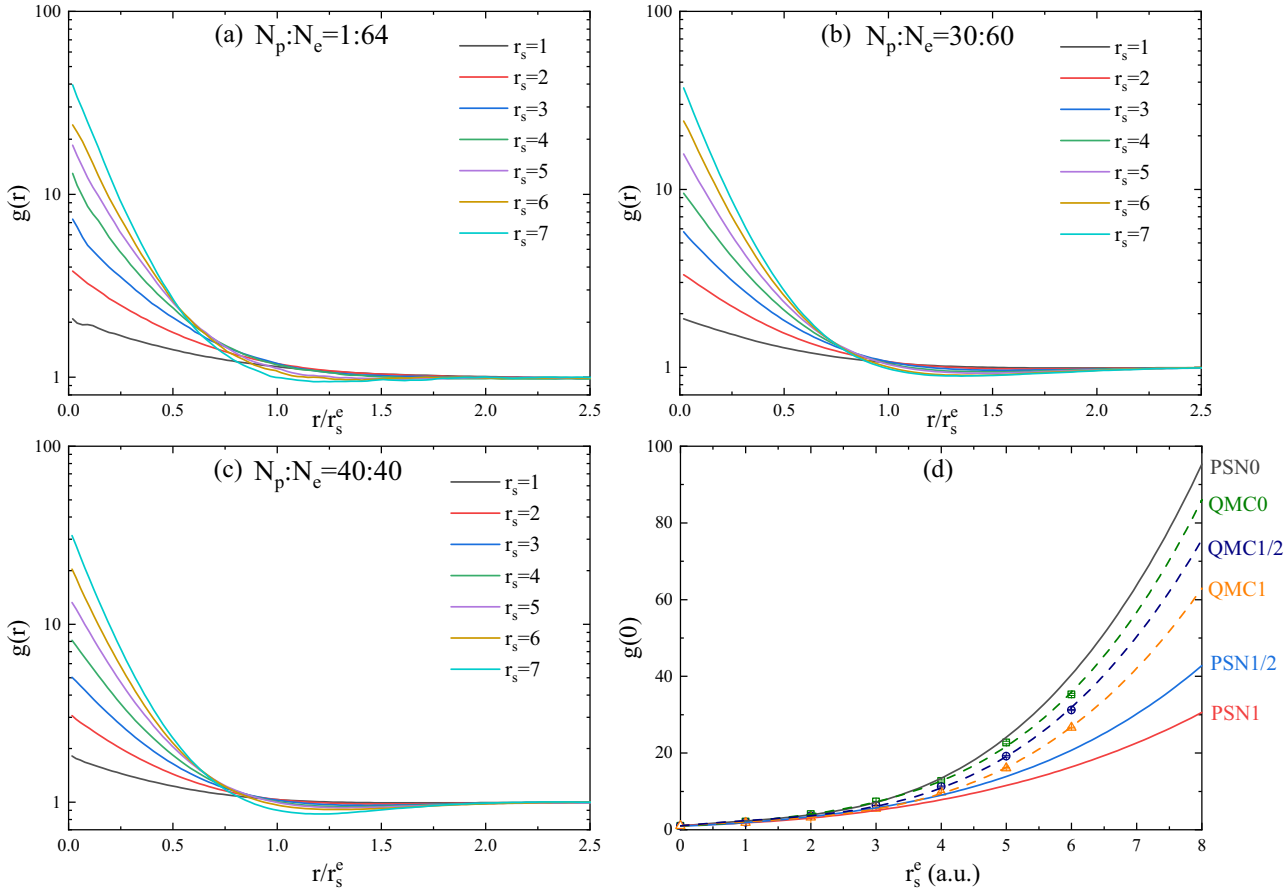

FIG. 1. PCF as a function of r/r_s^e for (a) $N_p : N_e = 1 : 64$, (b) $N_p : N_e = 30 : 60$, and (c) $N_p : N_e = 40 : 40$, calculated from DMC simulations with a time step of 0.001 a.u. (d) The $g(0)$ at three different density ratios derived from the PSN scheme and QMC simulations. The indexes of 0, 1, and 2 represent $R \to 0$ ($N_p : N_e = 1 : 64$), $R = 1$ ($N_p : N_e = 40 : 40$), and $R = 1/2$ ($N_p : N_e = 30 : 60$), respectively. The dashed lines are the fitted curves of data obtained from the QMC simulations. The solid lines are obtained from the PSN scheme.

TABLE II. The QMC simulations of correlation energy per volume, $E_{c,v}^{e-p}$, for different r_s^e values at $R = N_p/N_e = 1$ and $R = N_p/N_e = \frac{1}{2}$. The unit of the energy is 10^{-3} Rydberg per unit volume.

r_s^e	N_e	N_p	$E_{c,v}^{e-p}$ (mRy/a.u.)	Error of $E_{c,v}^{e-p}$ (mRy/a.u.)
1.0	40	40	−46.256	3.6718
1.2	40	40	−25.586	1.2489
1.4	40	40	−15.670	1.0440
2.0	40	40	−5.021	0.2459
3.0	40	40	−1.4203	0.0550
4.0	40	40	−0.6034	0.0311
5.0	40	40	−0.3231	0.0055
6.0	40	40	−0.2012	0.0023
7.0	40	40	−0.1320	0.0016
1.0	60	30	−31.101	3.9276
2.0	60	30	−3.372	0.2477
3.0	60	30	−0.950	0.0528
4.0	60	30	−0.401	0.0378
5.0	60	30	−0.212	0.0016
6.0	60	30	−0.130	0.0022
7.0	60	30	−0.086	0.0017

used to modify the potential energy within this range, while keeping the continuity at the boundary by making adjustments in ϵ_0, as clarified in Appendix C.

In summary, we use the QMC method to modify the formulas closely related to positrons in our calculations. Due to significant changes in the electron-positron correlation energy and enhancement factor, our final results show noticeable differences compared to the calculations before modification. The specific details of the calculations and the results are described in the subsequent sections.

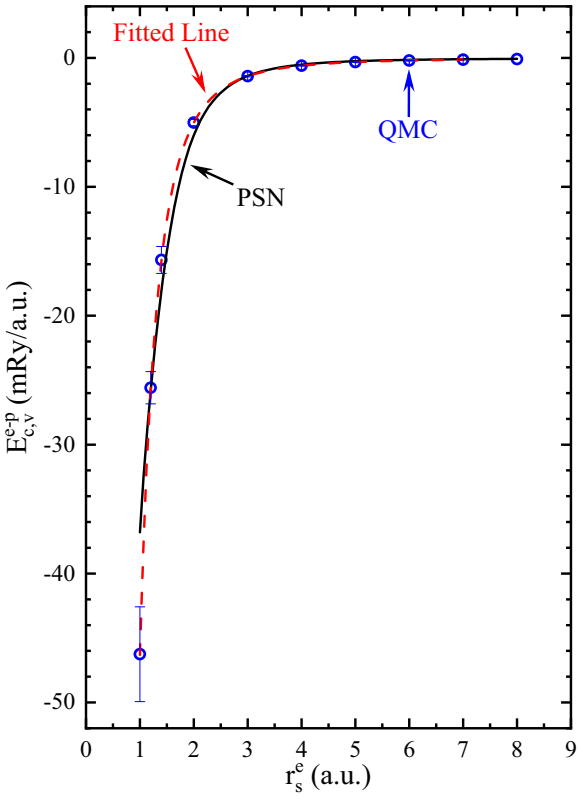

FIG. 2. The correlation energy obtained from QMC simulations at $R = 1$. The red dashed line is the curve fitted by the QMC data points using Eq. (15), and the black solid line is obtained from the PSN scheme. The unit of the energy is 10^{-3} Rydberg per unit volume.

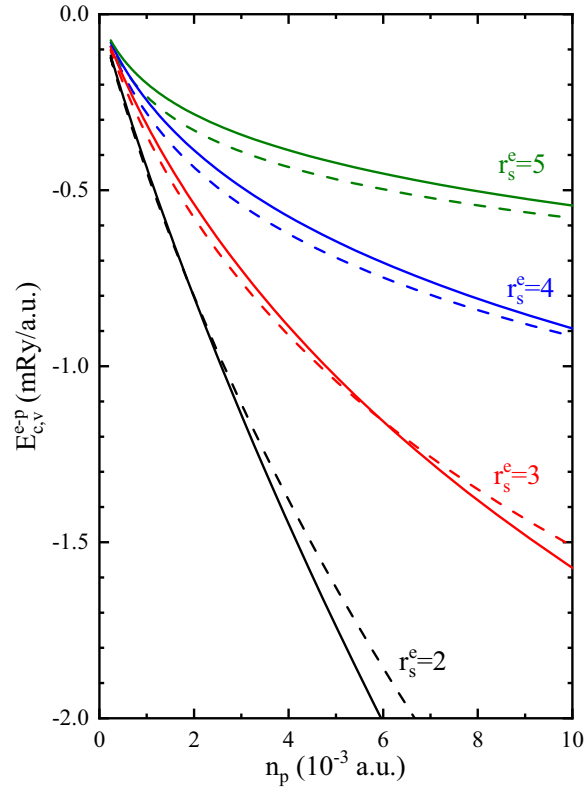

FIG. 3. The comparison between new correlation energy (dashed line) and PSN correlation energy (solid line) as a function of positron density n_p at $r_s^e = 2, 3, 4, 5$. The unit of the energy is 10^{-3} Rydberg per unit volume.

IV. CALCULATION DETAILS AND RESULTS

In practical applications, a fully self-consistent algorithm is employed to perform TCDFT calculations similar as described in Wiktor's excellent work [11] and the semiconductor corrections are not taken into account in the calculation. Since there is only one single positron in the system, self-interaction correction (SIC) has been done in ABINIT code so that there is no positron-positron Hartree and exchange-correlation interaction. The projector augmented-wave (PAW) approach is utilized [27] and semicore electrons were set to be valence electrons in the pseudopotentials that we used to ensure the positron wave function behaves well near the nucleus. The lattice parameters we used are experimental lattice parameters obtained through the Materials Project. The two-body self-consistent loop is shown in Fig. 4. It is convenient for us to utilize the the open-source software package ABINT [28,29]. In the full electron-positron correlation functional calculation of bulk lifetimes, we set the positron occupation to be 0.001 to make sure it can be close enough to the zero positron limit and we only take CONV instead of the self-consistent scheme. In the calculation of defect lifetimes, the self-consistent scheme is used and it is necessary to consider lattice relaxation to

TABLE III. Experimental bulk positron lifetimes of some materials.

Material	Expt.	Expt.*
Li	291 [33]	291
C-diamond	97.5 [34], 107 [35]	102
Na	338 [33]	338
Mg	220 [36], 225 [37]	223
Al	160.7 [38]	161
Si	216.7 [39], 217 [34], 218 [35]	217
Fe	108.0 [40]	108
Ni	104.3 [34]	104
Cu	112 [41]	112
Ga	198 [42]	198
Ge	222 [35], 228 [37], 228 [43]	226
Ag	130 [37]	130
Au	117 [44], 113 [45]	115
GaAs	231.6 [46], 231 [47], 230 [48]	231
MgO	130 [49], 166 [50], 152 [50], 155 [51]	151
ZnO	153 [52], 159 [53], 158 [54], 161 [55]	158
SiC-3C	138 [56], 140 [57]	139
NiO	110 [51]	110

accurately calculate the localized state of the positron. We calculated monovacancy defects of Si, Al, GaAs, ZnO, 3C-SiC, and MgO. We used 2×2×2 supercells for Si, GaAs, 3C-SiC, and MgO, while 3×3×3 supercells were used for Al and ZnO to ensure that there are at least 64 atoms in a supercell. The exchange-correlation (xc) functionals in the pseudopotential files are Perdew-Burke-Ernzerhof (PBE) generalized gradient approximation [30]. The results are shown in Table III, with results from other LDA schemes including Boronski-Nieminen LDA (BNLDA) [31], Arponen-Pajanne LDA (APLDA) [15], and perturbed-hypernetted-chain LDA (PHCLDA) [32].

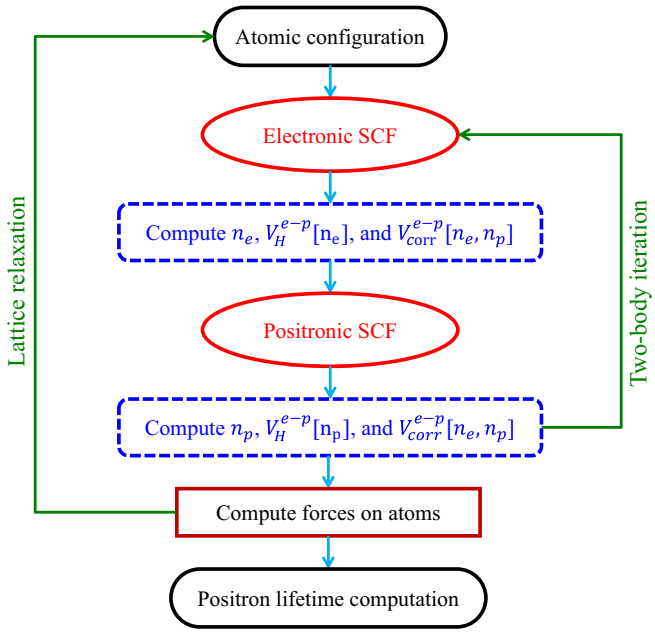

FIG. 4. A fully self-consistent TCDFT loop. V_H^{e-p} and $V_{\rm corr}^{e-p}$ refer to the electron-positron Hartree potential and correlation potential, respectively. $V_{\rm corr}^{e-p}$ and the enhancement factor used here are obtained from QMC simulations.

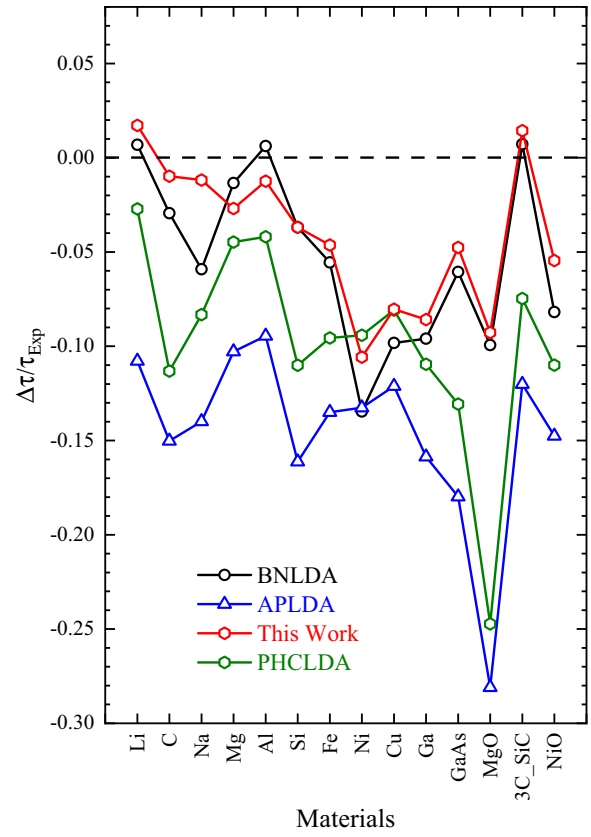

FIG. 5. The relative error $(\Delta\tau/\tau_{\rm Exp})$ between the four calculation results and the experimental values for the bulk positron lifetimes of some materials.

The experimental values of the bulk lifetimes are shown in Table III. These values are chosen from Campillo Roble's paper [58]. We try to choose the experimental values after 1990 and the statistical error smaller than 2 ps. If there are no such values, we then chose the latest values or the values with an error smaller than 5 ps after 1980. In Tables III and IV, we show the average experimental values. Figure 5 shows the relative errors $[(\tau - \tau_{\rm Exp}*)/\tau_{\rm Exp}*$, where τ is the computational value of a certain LDA scheme and $\tau_{\rm Exp}$ is the average of the experimental values] between the calculated values and experimental values of the lifetimes of various materials in Table III for different computational approaches. As a comparison, we directly used a zero-positron limit correlation functional to calculate the bulk lifetimes. We then compared these results with the calculations using the fully electron-positron correlation functional with positron occupancy set to 0.001. The comparison reveals that there is almost no difference between the two sets of results, demonstrating that setting the positron occupancy to 0.001 is sufficiently close to zero. Figure 6 represents the relative standard deviation of the each calculation scheme to judge which scheme is the best. From Fig. 5, our computational scheme generally underestimates the bulk lifetimes. From Fig. 6, we can tell that in terms of the calculated materials, our scheme performs the best.

TABLE IV. Bulk positron lifetimes of some materials from different calculation schemes and the number of valence electrons used in pseudopotential files. In the table, ZPL represents zero-positron limit, which means using a correlation functional within zero-positron limit directly, FC represents full correlation functional, which means using a full correlation functional in the calculation and setting the positron occupation to 0.001. The absolute deviation between the calculation values and average experimental values is shown in the parentheses after each calculation value.

		Positron annihilation lifetime (ps)					
Material	Valence No.	BNLDA	APLDA	PHCLDA	This work (ZPL)	This work (FC)	Expt.*
Li	3	293 (2)	260 (31)	283 (8)	296 (5)	296 (5)	291
C-diamond	4	99 (3)	87 (15)	90 (12)	101 (1)	101 (1)	102
Na	9	318 (20)	291 (47)	310 (28)	334 (4)	334 (4)	338
Mg	10	220 (3)	200 (23)	213 (10)	218 (5)	217 (6)	223
Al	11	162 (1)	146 (15)	154 (7)	159 (2)	159 (2)	161
Si	12	209 (8)	182 (35)	193 (24)	208 (9)	209 (8)	217
Fe	16	102 (6)	93 (15)	98 (10)	103 (5)	103 (5)	108
Ni	18	90 (14)	90 (14)	94(10)	93 (14)	93 (14)	104
Cu	19	101 (11)	98 (14)	103 (9)	103 (8)	103 (8)	112
Ga	21	179 (19)	167 (31)	176 (22)	180 (18)	181 (17)	198
GaAs	21 for Ga, 23 for As	217 (14)	189 (42)	201 (30)	219 (12)	220 (11)	231
MgO	10 for Mg, 6 for O	136 (15)	109 (42)	114 (37)	137 (14)	137 (14)	151
3C-SiC	12 for Si, 4 for C	140 (1)	122 (17)	129 (10)	142 (3)	141 (2)	139
NiO	18 for Ni, 6 for O	101 (9)	94 (16)	98 (12)	104 (6)	104 (6)	110

The primary goal of this work is to accurately calculate the positron annihilation lifetimes in vacancy-type defects. Indeed, for the case of positron localization within a vacancy, its density can reach a level comparable to the electron density in certain regions. In such cases, using the zero-positron-density approximation for calculations may have a significant deviation. Therefore, a fully self-consistent computational approach is a more reasonable choice in these situations. Due to the additional computational resources and time required for vacancy calculations, we choose only a few representative materials for which experimental values are reported, and we focus solely on calculating their monovacancy positron annihilation lifetimes. The results are shown in Table V.

Si is often used as a benchmark to assess the accuracy of computational schemes. Previous calculation schemes have successfully determined the positron annihilation lifetimes of monovacancy in Si [11]. Our calculations for both the bulk lifetime and monovacancy lifetime in Si are slightly smaller than the experimental results. Other computed values exhibit similar patterns as well. The computational results for aluminum (Al) are also 8 ps lower than the experimental values. Different papers present significant discrepancies in the computational results for the As monovacancy (V_{As}) in GaAs [9,47,64]. Our calculations indicate a positron lifetime of approximately 293 ps for V_{As} and 235 ps for V_{As}^{-}, which are more in line with the experimental analysis conducted by Saarinen *et al.* (295 ps for V_{As} and 257 ps for V_{As}^{-}) [47]. The calculation results of monovacancy V_{Si} with different charge states of 3C-SiC are slightly lower than the results of PSN (the PSN results here are smaller than the values in Wiktor's work [65] since we did not apply the semiconductor correction), but the differences are not substantial. Kerbiriou *et al.* did observe a signal varying with temperature from 210 to 220 ps [66]; our calculation results also support the inference that these

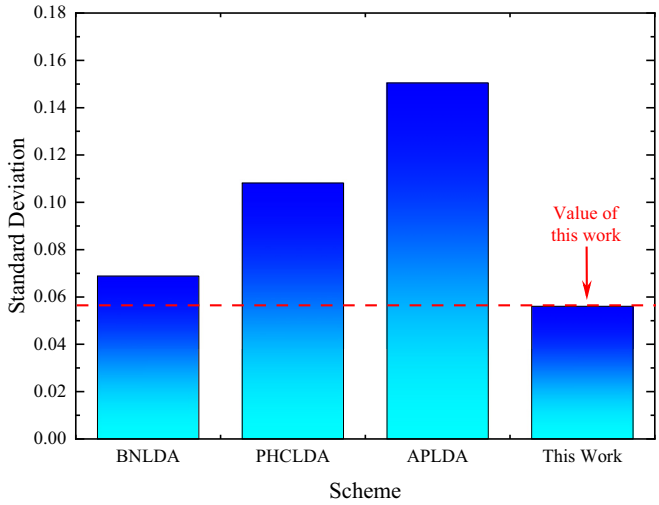

FIG. 6. The standard deviation of relative errors derived from Fig. 5.

TABLE V. The monovacancy lifetimes of some materials calculated by this computational scheme and PSN scheme.

	Positron Annihilation Lifetime (ps)		
	This work	PSN	Expt.
Si-V_{Si}	265	273	272 [59], 273 [60]
Al-V_{Al}	236	249	244 [61]
GaAs-V_{As}	293	310	295 [47]
GaAs-V_{As}^{-}	235	267	257 [47]
ZnO-V_{Zn}	221	229	230 [62]
3C-SiC-V_{Si}	213	220	210-220 [57]
3C-SiC-V_{Si}^{-}	210	217	210-220 [57]
3C-SiC-V_{Si}^{2-}	207	214	210-220 [57]
MgO-V_{Mg}	185	192	180 [49], 210 [63]

signals arise from different charge states of Si monovacancy defects. The result of V_{Zn} in ZnO is again smaller than the experimental data. In conclusion, both the bulk lifetimes and defect lifetimes calculated in our study are mostly smaller than the experimental results and the PSN scheme results, mostly because of our larger enhancement factor, which is consistent with the anticipated underestimation of lifetimes by LDA. However, the discrepancies are not outrageously large and our results demonstrate a certain degree of reasonability. In the future, we can adjust the LDA model using the GGA method, which will require further research to explore GGA corrections under finite densities. Our model holds the potential to provide computational values that are more consistent with experimental results.

V. CONCLUSION

In summary, a different calculation scheme was proposed after a series of QMC simulations to modify the electron-positron correlation energy and enhancement factor based on the formulas proposed by Puska *et al.* The new enhancement factor was generally larger than the previous value, especially in the calculation of vacancy-type defects. We took advantage of the open source package ABINIT to perform our calculation with the PAW approach. For the calculation of vacancy-type defects, lattice relaxation was considered.

This work demonstrates good overall agreement between the calculated and experimental values. For bulk lifetimes, our computation scheme yields better results compared to APLDA, PHCLDA, and BNLDA. For monovacancy defect lifetimes, our calculated values are generally lower compared to the results of the PSN scheme and experimental values. However, this does not imply that our results are worse. There is hope to obtain more precise computational values, after conducting study on GGA corrections in the future.

In conclusion, we proposed a different LDA scheme to calculate positron lifetimes, not only for bulk materials but also for vacancy-type defects.

ACKNOWLEDGMENTS

This work was financially supported by the National Key R&D Program of China (Grant No. 2019YFA0210000) and the National Natural Science Foundation of China (Grants No. 12175232, No. 11975225, and No. 12275270).

APPENDIX A: THE WAVE FUNCTION USED IN THE QMC CALCULATION AND THE FITTING OF THE CONTACT PCF

Since we only use the u term in the Jastrow optimization, the detailed expression of the wave function can be written as

$$\begin{aligned}
&\psi_{PW}^{SJ}(\mathbf{r'}_1, \mathbf{r'}_2, \ldots, \mathbf{r'}_{N_p}; \mathbf{r}_1, \mathbf{r}_2, \ldots, \mathbf{r}_{N_e}) \\
&= \exp\left[\sum_{I=1}^{N_p}\sum_{i=1}^{N_e} u_{ep}(|\mathbf{r}_i - \mathbf{r}_I|) + \sum_{i=1}^{N_{e\uparrow}-1}\sum_{j=i+1}^{N_{e\uparrow}} u_{\uparrow\uparrow}^{e}(|\mathbf{r}_i - \mathbf{r}_j|) + \sum_{i=N_{e\uparrow}+1}^{N_e-1}\sum_{j=i+1}^{N_e} u_{\uparrow\uparrow}^{e}(|\mathbf{r}_i - \mathbf{r}_j|) + \sum_{i=1}^{N_{e\uparrow}}\sum_{j=N_{e\uparrow}+1}^{N_e} u_{\uparrow\downarrow}^{e}(|\mathbf{r}_i - \mathbf{r}_j|)\right. \\
&\quad \left. + \sum_{I=1}^{N_{p\uparrow}-1}\sum_{J=I+1}^{N_{p\uparrow}} u_{\uparrow\uparrow}^{p}(|\mathbf{r'}_I - \mathbf{r'}_J|) + \sum_{I=N_{p\uparrow}+1}^{N_p-1}\sum_{J=I+1}^{N_p} u_{\uparrow\uparrow}^{p}(|\mathbf{r'}_I - \mathbf{r'}_J|) + \sum_{I=1}^{N_{p\uparrow}}\sum_{J=N_{p\uparrow}+1}^{N_p} u_{\uparrow\downarrow}^{p}(|\mathbf{r'}_I - \mathbf{r'}_J|)\right]\psi_s(\mathbf{r'}_1, \ldots, \mathbf{r'}_{N_p}; \mathbf{r}_1, \ldots, \mathbf{r}_{N_e}),
\end{aligned} \tag{A1}$$

where label e is for electron and label p is for positron; $N_e = N_{e\uparrow} + N_{e\downarrow}$ and $N_p = N_{p\uparrow} + N_{p\downarrow}$, where N_e and N_p are the total number of electrons and positrons. $\uparrow$ and $\downarrow$ are spin-up and spin-down particles. $\mathbf{r'}_I$ and $\mathbf{r}_i$ are the positions of positron I and electron i. ψ_s is the Slater wave function. And for two of the same kind of particles, we have $u_{\uparrow\uparrow} = u_{\downarrow\downarrow} \neq u_{\uparrow\downarrow}$.

Backflow corrections in QMC are capable of introducing further correlations in ψ^{SJ} by substituting the coordinates in the Slater determinants by a set of collective coordinates $\mathbf{x_i}(\{r_j\})$, given by

$$\mathbf{x}_i = \mathbf{r}_i + \xi_i(\{\mathbf{r}_j\}), \tag{A2}$$

where ξ_i is the backflow displacement of particle i, which depends on the configuration of the system $\{\mathbf{r}_j\}$, and contains optimizable parameters that can be fed into a standard method such as variance minimization.

As for the extracting of the contact PCFs, we first applied $2g_{\mathrm{DMC}} - g_{\mathrm{VMC}}$ to obtain $g(r)$. Then we fitted the polynomial $a_0 - r + a_2r^2 + a_3r^3 + a_4r^4 + a_5r^5 + a_6r^6 + a_7r^7$ to $\log[g(r)]$, where a_0, a_2, a_3, a_4, a_5, a_6, and a_7 are fitting parameters. The polynomial satisfies the Kimball cusp condition [26]. We choose a seventh-degree polynomial to enhance fitting accuracy while smoothing out the tail (r became large) as much as possible. Then the contact PCF is $g(0) = \exp(a_0)$. In order to obtain the errors on $g(0)$, the standard deviation of each bin of $g(r)$ data should be the same, and we calculate the χ^2 of the fit and make it equal to the degrees of freedom,

$$\chi^2 = \sum_{i=1}^{n} \frac{(O_i - C_i)^2}{\sigma^2} = n - 7, \tag{A3}$$

where n is the number of data, 7 is the number of fitting parameters, O_i is the data observed, C_i is the calculation value, and σ is the standard deviation. So the standard deviation should be

$$\sigma = \sqrt{\frac{\sum_{i=1}^{n}(O_i - C_i)^2}{n-7}}. \tag{A4}$$

Hence, we could determine the standard deviation in $g(0)$.

TABLE VI. Energy obtained by SJ and SJB through DMC.

r_s^e	$R=1/2$		$R=1$	
	E_{DMC}^{SJ}	$E_{\mathrm{DMC}}^{\mathrm{SJB}}$	E_{DMC}^{SJ}	$E_{\mathrm{DMC}}^{\mathrm{SJB}}$
1	0.4309	0.4286	0.4907	0.4884
2	−0.0548	−0.0568	−0.0527	−0.0546
3	−0.1073	−0.1086	−0.1129	−0.1146
4	−0.1130	−0.1145	−0.1208	−0.1226
5	−0.1106	−0.1121	−0.1194	−0.1212
6	−0.1070	−0.1087	−0.1169	−0.1190

APPENDIX B: THE FINITE-SIZE ERROR AND THE COMPARISON OF THE RESULTS OF SJ AND SJB OPTIMIZATION

The results of correlation energy and enhancement factors of SJ (Slater, Jastrow) and SJB (Slater, Jastrow and Backflow) optimization at $R=1/2$ and $R=1$ are shown in Table VI and Fig. 7, correspondingly. They show a significant level of consistency. Considering the smaller variance of the SJB wave function, we chose the results of SJB.

The finite-size error of the correlation energy and contact PCFs are ignored. The PCFs should be multiplied by $N_e/(N_e-1)$ according to Drummond's work [67], where N_e is the electron number. However, this will also violate the normalization condition on the finite-system PCF. Besides, the errors are even smaller than the difference between two QMC simulations with different time steps. So we just ignore the error brought by this correction in our contact PCFs. In Fig. 8, we have shown energy [Figs. 8(a) and 8(b)] and contact PCF [Figs. 8(c) and 8(d)] with different total particle numbers in simulation systems at $r_s^e=4$. The results remain consistent after the total number of particles larger than 60. Taking the energy, for example, the energy of different total particle numbers is shown in Fig. 8. The value of 80 particles for $R=1$ is −0.1223 Hartree/particle and for $R=\frac{1}{2}$ with 90 particles is −0.1144 Hartree/particle, and the errors after 64 particles are smaller than 3%. If we use Eq. (B1) [25] to do the correction, we will obtain −0.1205 Hartree/particle [red dashed line in Fig. 8(b)] and −0.1150 Hartree/particle [blue dashed line in Fig. 8(a)], which keeps the error smaller than 3%. N is the particle number, E_∞ is the energy of N particles system, ΔT_{HF} is the difference between the Hartree-Fock kinetic energies of the finite and infinite systems, and the term b/N accounts for the finite-size effects arising in the interaction energy. We find that this can be disregarded, especially for the lifetime calculation. The same situation applies to other simulations as well. So we decided to use the results without correction directly,

$$E_\infty = E_N + a\Delta T_{HF}(N) + \frac{b}{N}. \tag{B1}$$

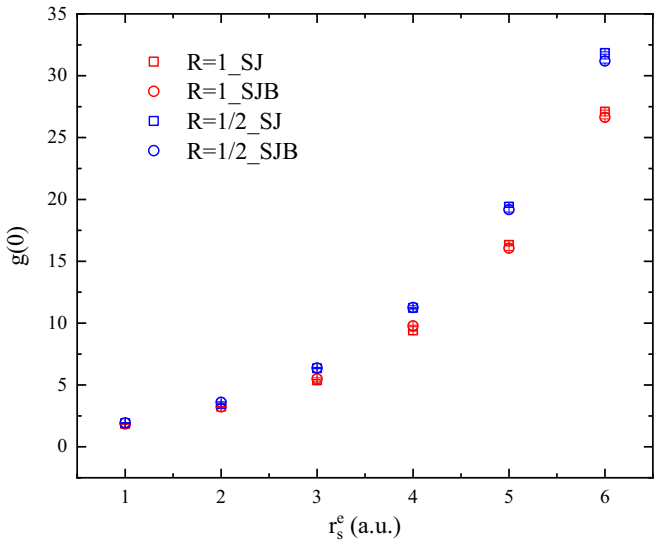

FIG. 7. The contact PCF obtained by SJ plane waves (square) and SJB plane waves (circle) at $R=1/2$ (blue) and $R=1$ (red).

APPENDIX C: ADJUSTMENTS IN ϵ_0

The correlation energy of one positron in homogeneous electron gas, ϵ_0, can be expressed as follows (in Ry) [8]:

For $r_s \leqslant 0.302$,

$$\epsilon = -1.56/\sqrt{r_s} + (0.051\ln r_s - 0.081)\ln r_s + 1.14. \tag{C1}$$

For $0.302 \leqslant r_s \leqslant 0.56$,

$$\epsilon = -0.92305 - \frac{0.05459}{r_s^2}. \tag{C2}$$

For $0.56 \leqslant r_s \leqslant 8.0$,

$$\epsilon = -\frac{13.15111}{(r_s+2.5)^2} + \frac{2.8655}{r_s+2.5} - 0.6298. \tag{C3}$$

For $8.0 \leqslant r_s \leqslant \infty$,

$$\epsilon = -179856.276\,8n^2 + 186.4207n - 0.524. \tag{C4}$$

Now, we need to replace the expression where $1 \leqslant r_s \leqslant 8$ by the formula obtained by Drummond *et al.* [14]. In order to keep the continuity of the derivatives and function values at $r_s=1$ and $r_s=8$, we add a term $\frac{0.092\,681\,3}{101}r_s^{101}$ to Eq. (C3) and $-3.386\,7\times10^7 n^3$ to Eq. (C4) to ensure the continuity of derivatives and then adjust the constants of all four expressions to ensure the continuity of function values. Two additional terms will quickly vanish when r_s is away from the two breakpoints $r_s=1$ and $r_s=8$.

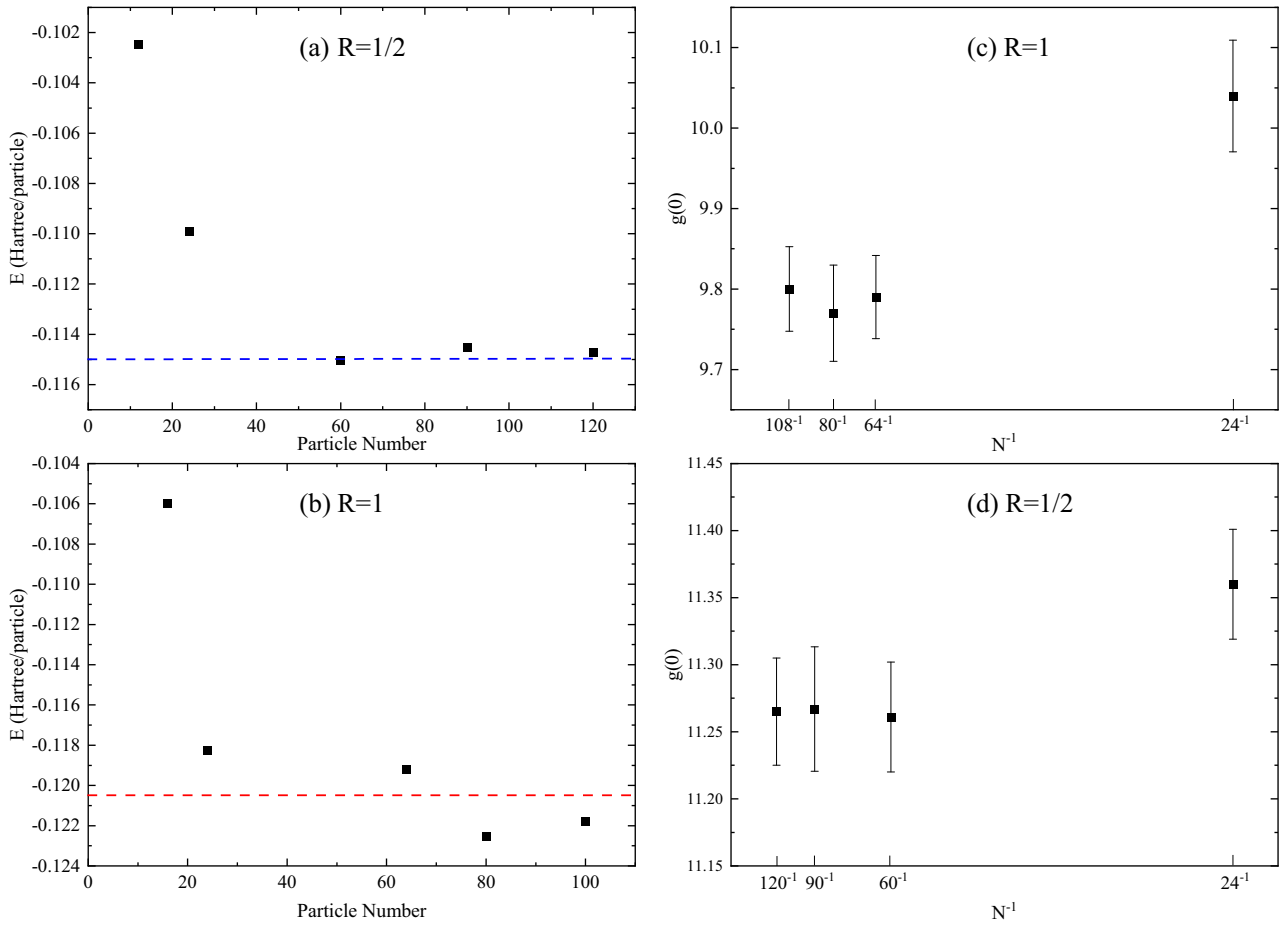

FIG. 8. The energy and $g(0)$ obtained by QMC simulations at (a),(d) $R = \frac{1}{2}$, $r_s^e = 4$ and (b),(c) $R = 1$, $r_s^e = 4$ with different total particle numbers. The blue and red dashed lines represent the values derived by Eq. (B1).

[1] P. Hautojärvi and C. Corbel, Positron spectroscopy of defects in metals and semiconductors, in *Positron Spectroscopy of Solids* (IOS Press, Amsterdam, Netherlands, 1995), pp. 491–532.

[2] J. Čížek, Characterization of lattice defects in metallic materials by positron annihilation spectroscopy: A review, J. Mater. Sci. Technol. **34**, 577 (2018).

[3] D. Bigg, A review of positron annihilation lifetime spectroscopy as applied to the physical aging of polymers, Polym. Eng. Sci. **36**, 737 (1996).

[4] D. Huang, Y. Dong, H. Guo *et al.*, Minute-scale evolution of free-volume holes in polyethylenes during the continuous stretching process observed by *in situ* positron annihilation lifetime experiments, Macromolecules **56**, 4748 (2023).

[5] M. J. Puska and R. M. Nieminen, Theory of positrons in solids and on solid surfaces, Rev. Mod. Phys. **66**, 841 (1994).

[6] F. Tuomisto and I. Makkonen, Defect identification in semiconductors with positron annihilation: Experiment and theory, Rev. Mod. Phys. **85**, 1583 (2013).

[7] R. M. Nieminen, E. Boronski, and L. J. Lantto, Two-component density-functional theory: Application to positron states, Phys. Rev. B **32**, 1377(R) (1985).

[8] E. Boroński and R. M. Nieminen, Electron-positron density-functional theory, Phys. Rev. B **34**, 3820 (1986).

[9] L. Gilgien, G. Galli, F. Gygi, and R. Car, *Ab initio* study of positron trapping at a vacancy in GaAs, Phys. Rev. Lett. **72**, 3214 (1994).

[10] M. J. Puska, A. P. Seitsonen, and R. M. Nieminen, Electron-positron Car-Parrinello methods: Self-consistent treatment of charge densities and ionic relaxations, Phys. Rev. B **52**, 10947 (1995).

[11] J. Wiktor, G. Jomard, and M. Torrent, Two-component density functional theory within the projector augmented-wave approach: Accurate and self-consistent computations of positron lifetimes and momentum distributions, Phys. Rev. B **92**, 125113 (2015).

[12] J. Arponen and E. Pajanne, Electron liquid in collective description. III. Positron annihilation, Ann. Phys. **121**, 343 (1979).

[13] L. J. Lantto, Variational theory of multicomponent quantum fluids: An application to positron-electron plasmas at $T = 0$, Phys. Rev. B **36**, 5160 (1987).

[14] N. D. Drummond, P. Lopez Ríos, R. J. Needs, and C. J. Pickard, Quantum Monte Carlo study of a positron in an electron gas, Phys. Rev. Lett. **107**, 207402 (2011).

[15] B. Barbiellini, M. J. Puska, T. Torsti, and R. M. Nieminen, Gradient correction for positron states in solids, Phys. Rev. B **51**, 7341 (1995).

[16] J. Kuriplach and B. Barbiellini, Gradient correction scheme for bulk and defect positron states in materials: New developments, J. Phys.: Conf. Ser. **505**, 012040 (2014).
[17] W. Zhang, B. Gu, J. Liu, and B. Ye, Accurate theoretical prediction on positron lifetime of bulk materials, Comput. Mater. Sci. **105**, 32 (2015).
[18] K. A. Simula, J. E. Muff, I. Makkonen, and N. D. Drummond, Quantum Monte Carlo study of positron lifetimes in solids, Phys. Rev. Lett. **129**, 166403 (2022).
[19] L. Deng, Y. Yuan, F. L. Pratt, W. Zhang, Z. Pan, and B. Ye, Two-component density functional theory study of quantized muons in solids, Phys. Rev. B **107**, 094433 (2023).
[20] R. Needs, M. Towler, N. Drummond, P. Lopez Rios, and J. Trail, Variational and diffusion quantum Monte Carlo calculations with the CASINO code, J. Chem. Phys. **152**, 154106 (2020).
[21] J. Kuriplach and B. Barbiellini, Improved generalized gradient approximation for positron states in solids, Phys. Rev. B **89**, 155111 (2014).
[22] Y. Kwon, D. M. Ceperley, and R. M. Martin, Effects of backflow correlation in the three-dimensional electron gas: Quantum Monte Carlo study, Phys. Rev. B **58**, 6800 (1998).
[23] P. Lopez Ríos, A. Ma, N. D. Drummond, M. D. Towler, and R. J. Needs, Inhomogeneous backflow transformations in quantum Monte Carlo calculations, Phys. Rev. E **74**, 066701 (2006).
[24] C. J. Umrigar, J. Toulouse, C. Filippi, S. Sorella, and R. G. Hennig, Alleviation of the fermion-sign problem by optimization of many-body wave functions, Phys. Rev. Lett. **98**, 110201 (2007).
[25] I. Gurtubay, R. Gaudoin, and J. M. Pitarke, Benchmark quantum Monte Carlo calculations of the ground-state kinetic, interaction and total energy of the three-dimensional electron gas, J. Phys.: Condens. Matter **22**, 065501 (2010).
[26] J. Kimball, Short-range correlations and electron-gas response functions, Phys. Rev. A **7**, 1648 (1973).
[27] M. Torrent, F. Jollet, F. Bottin, G. Zérah, and X. Gonze, Implementation of the projector augmented-wave method in the ABINIT code: Application to the study of iron under pressure, Comput. Mater. Sci. **42**, 337 (2008).
[28] X. Gonze, B. Amadon, G. Antonius *et al.*, The Abinit project: Impact, environment and recent developments, Comput. Phys. Commun. **248**, 107042 (2020).
[29] A. H. Romero, D. C. Allan, B. Amadon *et al.*, ABINIT: Overview, and focus on selected capabilities, J. Chem. Phys. **152**, 124102 (2020).
[30] J. P. Perdew, K. Burke, and M. Ernzerhof, Generalized gradient approximation made simple, Phys. Rev. Lett. **77**, 3865 (1996).
[31] M. J. Puska, S. Mäkinen, M. Manninen, and R. M. Nieminen, Screening of positrons in semiconductors and insulators, Phys. Rev. B **39**, 7666 (1989).
[32] H. Stachowiak and J. Lach, Positron-annihilation characteristics in an electron gas from low to high densities, Phys. Rev. B **48**, 9828 (1993).
[33] H. Weisberg and S. Berko, Positron lifetimes in metals, Phys. Rev. **154**, 249 (1967).
[34] Y. Li, S. Berko, and A. P. Mills, Positron lifetime in synthetic diamond, in *Materials Science Forum* (Trans Tech, Stafa-Zurich, Switzerland, 1992), Vol. 105, pp. 739–742.
[35] S. Dannefaer, W. Puff, and D. Kerr, Positron line-shape parameters and lifetimes for semiconductors: Systematics and temperature effects, Phys. Rev. B **55**, 2182 (1997).
[36] P. Hautojärvi, J. Johansson, A. Vehanen, J. Yli-Kauppila, J. Hillairet, and P. Tzanétakis, Trapping of positrons at vacancies in magnesium, Appl. Phys. A **27**, 49 (1982).
[37] M. Monge and J. Del Rio, Position annihilation in Kapton source-supporting foils, J. Phys.: Condens. Matter **6**, 2643 (1994).
[38] J. Čížek, I. Procházka, T. Kmječ, and P. Vostrý, Using of modified trapping model in positron-lifetime study of cold-worked aluminium, Phys. Status Solidi (a) **180**, 439 (2000).
[39] J. Makinen, P. Hautojarvi, and C. Corbel, Positron annihilation and the charge states of the phosphorus-vacancy pair in silicon, J. Phys.: Condens. Matter **4**, 5137 (1992).
[40] J. Čížek, I. Prochazka, J. Kočík, and E. Keilova, Positron lifetime study of reactor pressure vessel steels, Phys. Status Solidi (a) **178**, 651 (2000).
[41] K. Jensen, M. Eldrup, S. Linderoth, and J. Evans, Influence of krypton physisorption on the positron surface state lifetime: Rates of positron trapping into cavities, J. Phys.: Condens. Matter **2**, 2081 (1990).
[42] N. de Diego, J. del Rio, P. Moser, and F. Plazaola, Positron trapping at vacancies in Ga, J. Phys.: Condens. Matter **4**, 5037 (1992).
[43] M. Alatalo, B. Barbiellini, M. Hakala, H. Kauppinen, T. Korhonen, M. J. Puska, K. Saarinen, P. Hautojärvi, and R. M. Nieminen, Theoretical and experimental study of positron annihilation with core electrons in solids, Phys. Rev. B **54**, 2397 (1996).
[44] H. E. Schaefer, W. Stuck, F. Banhart, and W. Bauer, Thermal vacancies in the noble metals Cu, Ag, Au and in Pt studied by positron lifetime spectroscopy, in *Materials Science Forum* (Trans Tech, Stafa-Zurich, Switzerland, 1987), Vol. 15, pp. 117–124.
[45] C. Corbel, M. Stucky, and P. Moser, Positron lifetimes in vacancy type defects after electron irradiation in metals and semi-conductors, Ann. Chim. (Paris) **10**, 733 (1985).
[46] Z. Wang, S. Wang, Z. Chen, L. Ma, and S. Li, Defect properties in plastically deformed p-GaAs studied by positron lifetime measurements, Phys. Status Solidi (a) **177**, 341 (2000).
[47] K. Saarinen, P. Hautojärvi, P. Lanki, and C. Corbel, Ionization levels of As vacancies in as-grown GaAs studied by positron-lifetime spectroscopy, Phys. Rev. B **44**, 10585 (1991).
[48] A. Polity, F. Rudolf, C. Nagel, S. Eichler, and R. Krause-Rehberg, Defects in electron-irradiated GaAs studied by positron lifetime spectroscopy, Phys. Rev. B **55**, 10467 (1997).
[49] M. Mizuno, Y. Inoue, K. Sugita *et al.*, Positron annihilation study of formation of Mg vacancy in MgO, in *Materials Science Forum* (Trans Tech, Stafa-Zurich, Switzerland, 2004), Vol. 445, pp. 153–155.
[50] A. A. Valeeva, A. A. Rempel, W. Sprengel, and H.-E. Schaefer, Vacancies on the Ti sublattice in titanium monoxide TiO_y studied using positron annihilation techniques, Phys. Rev. B **75**, 094107 (2007).
[51] B. Barbiellini, P. Genoud, and T. Jarlborg, Calculation of positron lifetimes in bulk materials, J. Phys.: Condens. Matter **3**, 7631 (1991).

[52] M. Mizuno, H. Araki, and Y. Shirai, Theoretical calculations of positron lifetimes for metal oxides, Mater. Trans. **45**, 1964 (2004).

[53] G. Brauer, W. Anwand, W. Skorupa, J. Kuriplach, O. Melikhova, C. Moisson, H. von Wenckstern, H. Schmidt, M. Lorenz, and M. Grundmann, Defects in virgin and n^+-implanted ZnO single crystals studied by positron annihilation, Hall effect, and deep-level transient spectroscopy, Phys. Rev. B **74**, 045208 (2006).

[54] A. Uedono, T. Koida, A. Tsukazaki, M. Kawasaki, Z. Chen, S. Chichibu, and H. Koinuma, Defects in ZnO thin films grown on $ScAlMgO_4$ substrates probed by a monoenergetic positron beam, J. Appl. Phys. **93**, 2481 (2003).

[55] S. Brunner, W. Puff, A. G. Balogh, and P. Mascher, Characterization of radiation-induced defects in ZnO probed by positron annihilation spectroscopy, in *Materials Science Forum* (Trans Tech, Zurich-Uetikon, Switzerland, 2001), Vol. 363, pp. 141–143.

[56] G. Brauer, W. Anwand, E.-M. Nicht, J. Kuriplach, M. Šob, N. Wagner, P. G. Coleman, M. J. Puska, and T. Korhonen, Evaluation of some basic positron-related characteristics of SiC, Phys. Rev. B **54**, 2512 (1996).

[57] A. Kawasuso, H. Itoh, N. Morishita, M. Yoshikawa, T. Ohshima, I. Nashiyama, S. Okada, H. Okumura, and S. Yoshida, Silicon vacancies in 3C-SiC observed by positron lifetime and electron spin resonance, Appl. Phys. A: Mater. Sci. Process. **67**, 209 (1998).

[58] J. Campillo Robles and F. Plazaola, Collection of data on positron lifetimes and vacancy formation energies of the elements of the periodic table, in *Defect and Diffusion Forum* (Trans Tech, Stafa-Zurich, Switzerland, 2003), Vol. 213, p. 141.

[59] I. Makkonen, M. Hakala, and M. J. Puska, Modeling the momentum distributions of annihilating electron-positron pairs in solids, Phys. Rev. B **73**, 035103 (2006).

[60] J. Mäkinen, C. Corbel, P. Hautojärvi, P. Moser, and F. Pierre, Positron trapping at vacancies in electron-irradiated Si at low temperatures, Phys. Rev. B **39**, 10162 (1989).

[61] M. J. Fluss, L. C. Smedskjaer, M. K. Chason, D. G. Legnini, and R. W. Siegel, Measurements of the vacancy formation enthalpy in aluminum using positron annihilation spectroscopy, Phys. Rev. B **17**, 3444 (1978).

[62] F. Tuomisto, V. Ranki, K. Saarinen, and D. C. Look, Evidence of the Zn vacancy acting as the dominant acceptor in *n*-type ZnO, Phys. Rev. Lett. **91**, 205502 (2003).

[63] J. Xu, A. P. Mills Jr., A. Ueda, D. O. Henderson, R. Suzuki, and S. Ishibashi, Vacancy clusters on surfaces of Au nanoparticles embedded in MgO, Phys. Rev. Lett. **83**, 4586 (1999).

[64] S. Huang, J. Liu, and B. Ye, Investigation and calculation of positron lifetimes of monovacancies in crystals, J. Phys.: Conf. Ser. **674**, 012022 (2016).

[65] J. Wiktor, G. Jomard, M. Torrent, and M. Bertolus, Electronic structure investigation of energetics and positron lifetimes of fully relaxed monovacancies with various charge states in 3C-SiC and 6H-SiC, Phys. Rev. B **87**, 235207 (2013).

[66] X. Kerbiriou, M.-F. Barthe, S. Esnouf, P. Desgardin, G. Blondiaux, and G. Petite, Silicon displacement threshold energy determined by electron paramagnetic resonance and positron annihilation spectroscopy in cubic and hexagonal polytypes of silicon carbide, J. Nucl. Mater. **362**, 202 (2007).

[67] N. D. Drummond, P. Lopez Ríos, C. J. Pickard, and R. J. Needs, First-principles method for impurities in quantum fluids: Positron in an electron gas, Phys. Rev. B **82**, 035107 (2010).